https://doi.org/10.31436/iiumej.v27i2.4068

Design Optimization and Structural Evaluation of a Hybrid Frame for Next-Generation Electric Scooters

SRIDHAR R[1*], MAHANTESH M MATH[1], SUJAN CHAKRABORTY[1], SOURABHA H[1], VIVEKANAND S GOGI[2], JEEVATHITH R[1]

[1]*Department of Mechanical Engineering, R V College of Engineering, Bangalore, 560059, India*
[2]*Department of Industrial Engineering & Management, R V College of Engineering, Bangalore, 560059, India*

**Corresponding author: sridharr@rvce.edu.in*

(Received: 27 November 2025; Accepted: 2 February 2026; Published online: 10 May 2026)

ABSTRACT: The increasing adoption of electric scooters has introduced unique challenges in chassis design, where packaging constraints imposed by predefined outer shells often conflict with structural efficiency. This study presents the conceptual design, structural analysis, and validation of a hybrid chassis tailored for an electric scooter within such constraints. The frame integrates a step-through central region with a trellis-inspired rear subframe and a reinforced headstock. Three design iterations were modeled in SolidWorks and evaluated using finite element analysis (ANSYS) for static loads (1–3G), fatigue under cyclic loading, equivalent static impact loads, and modal behavior. Analytical stress checks and literature comparisons supported the simulations. Under 3G static loading, the final steel frame exhibited a maximum deformation of 3.16 mm with a minimum factor of safety of 1.48. Fatigue analysis predicted a life of 1.75×10^6 cycles, while modal analysis confirmed the first natural frequency at 28.56 Hz, above the expected excitation frequencies, and thus free from resonance. Although crash simulations showed localized yielding in severe impacts, the frame maintained integrity under operational conditions. These findings demonstrate that high structural performance can be achieved within strictly styling-defined packaging envelopes, validating the hybrid trellis–step-through configuration for electric scooters.

ABSTRAK: Peningkatan penggunaan skuter elektrik telah menyebabkan cabaran unik pada reka bentuk casis, di mana kekurangan pada pembungkusan, yang ditentukan oleh struktur luaran, sering bercanggah dengan kecekapan struktur. Kajian ini membentangkan reka bentuk konseptual, analisis struktur, dan pengesahan bagi casis hibrid yang direka khusus untuk skuter elektrik. Rangka casis ini mengintegrasi bahagian tengah jenis telus langkah dengan subrangka belakang berinspirasi jalaran serta stok kepala yang diperkukuh. Tiga iterasi reka bentuk dimodel menggunakan SolidWorks dan dinilai melalui analisis unsur terhingga menggunakan ANSYS bagi beban statik (1–3G), keletihan di bawah beban berkitar, beban impak statik setara, serta tingkah laku mod. Pengesahan analitikal terhadap tegasan serta perbandingan dengan kajian terdahulu turut menyokong dapatan simulasi. Di bawah beban statik 3G, rangka keluli akhir menunjukkan ubah bentuk maksimum sebanyak 3.16 mm dengan faktor keselamatan minimum 1.48. Analisis keletihan meramalkan jangka hayat sebanyak 1.75×10^6 kitaran, manakala analisis mod mengesahkan frekuensi asli pertama pada 28.56 Hz, iaitu melebihi frekuensi yang diuji dan bebas resonans. Walaupun simulasi perlanggaran menunjukkan luluh setempat di bawah impak teruk, rangka masih kukuh ketika beroperasi. Dapatan ini menunjukkan bahawa prestasi struktur yang tinggi boleh dicapai dalam persekitaran pembungkusan yang ketat berasaskan reka bentuk estetik, sekaligus mengesahkan keberkesanan konfigurasi hibrid jalaran–telus langkah pada skuter elektrik.

https://doi.org/10.31436/iiumej.v27i2.4068

KEYWORDS: *Electric scooter, hybrid chassis, trellis frame, finite element analysis, packaging constraints.*

1. INTRODUCTION

The structural design of two-wheeler chassis has long been explored in the motorcycle domain, where frame types such as double-cradle, backbone, perimeter, monocoque, and trellis layouts have undergone extensive optimization. Among these, the trellis frame has emerged as particularly effective, offering high torsional rigidity with relatively low material use due to its triangulated geometry [1]. In parallel, suspension design plays a critical role in handling and load transfer, and foundational studies on chassis–suspension interaction have provided a strong basis for modern two-wheeler development [2]. In contrast, scooter chassis design has historically been dominated by step-through and underbone configurations, which prioritize ease of use and compactness. While effective for urban commuting, these layouts inherently feature interrupted load paths that reduce stiffness and fatigue resistance compared to motorcycle frames [3]. The removal of the engine block further eliminates a key contributor to stiffness, while the introduction of bulky batteries and hub motors alters weight distribution and packaging constraints, complicating the design process. Computational design and stress analysis methods have shown potential in identifying safe stress limits and optimizing weight distribution for electric motorcycle frames [4]. Similar approaches applied to electric bike chassis have demonstrated how finite element simulations improve durability while supporting lightweighting goals [5]. Together, these studies highlight the growing importance of simulation in guiding structural design decisions for two-wheelers.

The transition to electric scooters introduces additional structural challenges. Manufacturers often impose styling envelopes that constrain frame geometries, forcing designers to balance accessibility with rigidity. To address this, researchers have proposed hybrid frame concepts that integrate scooter ergonomics with trellis-inspired geometries. Shivhare et al. [6] modeled a compact, lightweight scooter using finite element analysis, highlighting how triangulated layouts reduce weight without sacrificing stiffness. Goh and Chun [7] further advanced this idea by applying trellis-frame principles to electric scooters, demonstrating measurable improvements in both structural efficiency and vibration safety. Virtual evaluation methods now play a central role in validating chassis configurations. Finite Element Analysis (FEA) enables simulation of static loads, fatigue conditions, impact scenarios, and modal responses, offering a comprehensive framework for performance evaluation. Karthik [8] emphasized the value of simplified fabrication combined with reinforced member placement, achieving safety margins above 2.0 without excessive material use. Ajhay Babu [9] conducted a computational study of an electric two-wheeler frame, highlighting the importance of assessing natural frequencies and validating crashworthiness across multiple load cases.

Material optimization has also emerged as a decisive factor in electric vehicle chassis design. Charkha et al. [10] conducted a comparative analysis of materials for a three-wheeled electric vehicle, concluding that while composites offer lightweighting, structural steels provide higher fatigue safety margins under urban use. Rahmadi and Mursalin [11] analyzed a chopper-style motorcycle frame, reinforcing the importance of member geometry in achieving high durability and improved rider safety. Beyond conventional motorcycles, several studies have focused on small-format electric two-wheelers. Srinu et al. [12] applied computational analysis to an electric bike chassis, demonstrating how load-bearing components can be optimized for stiffness while reducing material consumption. Teja et al. [13] developed an

https://doi.org/10.31436/iiumej.v27i2.4068

electric moped chassis, emphasizing packaging efficiency and component integration within tight geometric envelopes. Vashist et al. [14] investigated electric two-wheeler frames under variable loading conditions, confirming the critical role of frame geometry in determining structural reliability. Biswal et al. [15] introduced an innovative sliding-frame electric bike design, showcasing adaptability and improved load management compared to fixed-frame configurations.

Taken together, these studies emphasize the need to integrate material selection, structural layout, fatigue validation, modal assessment, and manufacturability into a cohesive framework for electric scooter design. Despite these advances, hybrid trellis–step-through architectures remain underexplored. The present work addresses this gap by developing and analyzing such a chassis through virtual structural evaluation, aiming to balance accessibility, safety, and performance in urban mobility.

2. MATERIALS AND METHODOLOGY

2.1. Requirement Analysis

The chassis was designed to meet the performance needs of an urban step-through electric scooter while staying within the predefined packaging and ergonomic limits. Key requirements included a maximum payload capacity of 150 kg (rider, pillion, and luggage) plus an additional 30 kg for the motor and battery assembly. For Indian road conditions, the scooter required a minimum ground clearance of 150 mm and a wheelbase of about 1290 mm. The primary use case was daily urban commuting, in which the frame would be subjected to repeated loading from speed breakers, potholes, and surface irregularities. These parameters formed the basis for geometry design, material selection, and structural validation.

2.2. Body Shell Constraint Modeling

A 3D CAD model of the scooter's body shell was created in Autodesk Alias to serve as the primary packaging envelope for the chassis. The packaging model, shown in Figure 1a, defined the maximum permissible volume for structural members while preserving the step-through clearance essential for rider ergonomics. Mounting zones for key subsystems, such as the battery, motor, and suspension, were incorporated to facilitate integration.

Figure 1. (a) Chassis Packaging Model (b) Outer Body Shell

The outer body shell, shown in Figure 1b, imposed strict spatial limitations, particularly around the headstock, footboard, and seat regions, disrupting conventional load paths and restricting standard triangulated layouts. Consequently, the chassis geometry was developed to

fit within these allowable regions, balancing packaging constraints and structural efficiency. Dimensional limits included a total length of approximately 1900 mm, a wheelbase of roughly 1290 mm, and a minimum ground clearance of 185 mm.

2.3. Geometrical Modeling of Chassis

The chassis was developed using the CAD software (SolidWorks) in a packaging-driven approach, with a fixed body shell geometry serving as the governing design envelope. The objective was to integrate a structurally efficient hybrid step-through and trellis frame within the constrained volume while maintaining ergonomics, manufacturability, and serviceability.

The frame was divided into three functional zones. The front headstock region comprised a curved loop tube reinforced with gusseted members to carry steering and impact loads. The central spine and floorboard zone supported the battery and rider loads through larger-diameter 26.9 mm tubes. The rear subframe and swingarm mount were designed as a triangulated trellis structure to resist propulsion and suspension forces while providing impact absorption.

Table 1. Tube Profiles of Chassis

Sl. No	Tube size	Application zone
1	Ø33.7 mm × 2 mm	Headstock and frontal loop members
2	Ø26.9 mm × 2 mm	Main spine and floor support tubes
3	Ø21.3 mm × 2 mm	Secondary supports and rear triangulation

Circular steel tubes of Ø33.7 mm, Ø26.9 mm, and Ø21.3 mm with 2 mm wall thicknesses listed in Table 1 were employed. This configuration balanced stiffness and weight, resulting in an approximately 20 kg total assembly including brackets and welds. For preliminary member sizing validation, a 3G design case was considered using the scooter's gross design mass of 250 kg, including the rider, frame, and battery. This corresponds to a total vertical force given by Eq. (1).

$$F = nmg \tag{1}$$

where $n = 3$ is the load factor for the 3G design case, $m = 250$ kg, and $g = 9.81$ m/s^2. Thus, $F = 7357.5$ N. With an assumed moment arm of L=150 mm, the bending moment (M) was computed using Eq. (2)

$$M = FL \tag{2}$$

With $M = 1103.6$ Nm, for a Ø26.9 mm tube with 2 mm wall thickness, the inner diameter is $d = D - 2t = 22.9$ mm. The second moment of area, I, for a hollow circular tube, is given by $I = \frac{\pi}{64}(D^4 - d^4)$. The corresponding section modulus (S) is calculated using Eq. (3)

$$S = \frac{I}{D/2} = \frac{\pi}{32}\left(\frac{D^4 - d^4}{D}\right) \tag{3}$$

For $D = 26.9$ mm and $d = 22.0$ mm, then $S = 907.3$ mm^3. The bending stress (σ) was then calculated using Eq. (4)

$$\sigma = \frac{M}{S} \tag{4}$$

Using $M = 1103.6\ N \cdot m = 1.1036 \times 10^6 N.mm$, $\sigma = \frac{1.1046 \times 10^6}{907.33} = 1216.4$ MPa.

This bending stress exceeds the 350 MPa yield strength of E350 steel if the Ø26.9 mm tube is assumed to act as a single isolated member under the full 3G load. However, in the actual frame, the load is distributed among multiple interconnected members and further

supported by welded joints and triangulated structural paths. Therefore, this simplified calculation represents a conservative single-member validation case rather than the actual stress state of the complete frame.

Three CAD iterations were assessed to optimize structural performance. Iteration 1 employed a minimal bracing layout with a single central spine, but offered limited rigidity. Iteration 2 introduced frontal reinforcement and partial rear bracing, which improved stiffness yet still lacked mid-span support. Iteration 3, the final design, featured a fully triangulated rear trellis, multiple frontal braces, and gusset reinforcements, delivering the best balance of stiffness, weight, and manufacturability, and was therefore chosen for further analysis.

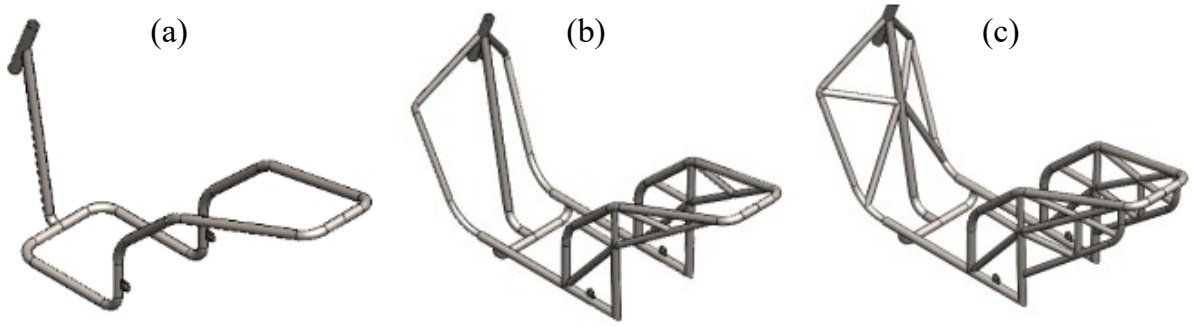

Figure 2. (a) 1st Chassis Iteration, (b) 2nd Chassis Iteration (c) 3rd Chassis Iteration

The final line sketch in Figure 3(a) confirmed key handling parameters: headstock angle 21.5°, wheelbase 1282 mm, trail 90.6 mm, and the center of gravity ~437 mm above ground. Footboard clearance was 232 mm, sufficient for Indian urban road conditions. These values were carried over into the CAD model (Figure 3(b)) for subsequent simulation.

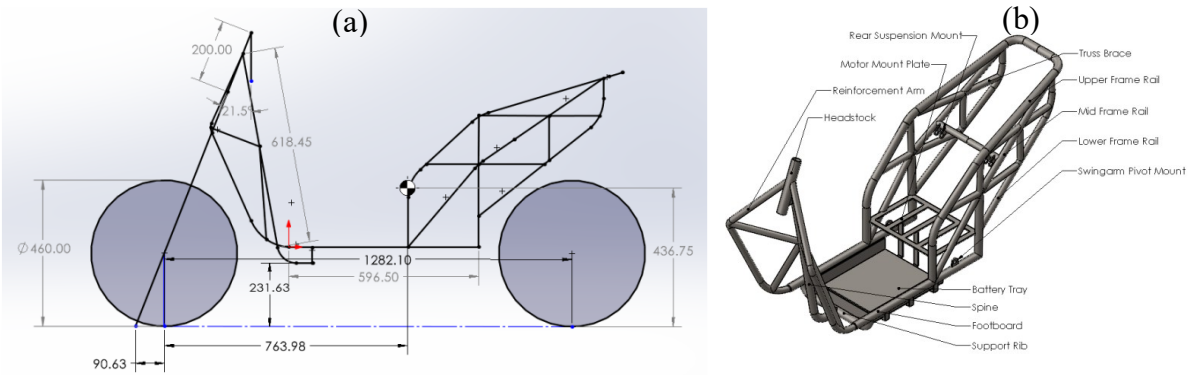

Figure 3. (a) Final Chassis Geometry Line Sketch (b) Final Chassis Assembly

A non-functional scaled 3D-printed model was fabricated using fused deposition modeling (FDM) for design communication and ergonomic validation (Figure 4). The chassis was printed in PLA to represent structural members, while the body shell was printed in a contrasting color to illustrate packaging compliance.

https://doi.org/10.31436/iiumej.v27i2.4068

Figure 4. Scaled 3D-printed models of (a) hybrid trellis chassis and (b) complete scooter with a body shell.

2.4. Material Selection

The choice of frame material plays a critical role in ensuring structural stiffness, fatigue resistance, manufacturability, and cost-effectiveness. Since the chassis must withstand both static and dynamic urban loads, a performance-based selection methodology was employed using Ashby material indices (Figure 5a). The key requirements for selection included stiffness to minimize deformation under operational loads, strength to prevent yielding and fatigue failure, manufacturability in terms of weldability, tube availability, and ease of fabrication, and cost-effectiveness for large-scale production. Based on these criteria, three candidate materials were shortlisted: AISI 4130 Chromoly steel, which offers high strength and excellent fatigue resistance; IS 2062 E350 structural steel, which provides moderate strength, good availability, and is highly economical; and Aluminum 6061-T6, which is lightweight, corrosion-resistant, and already widely used in electric vehicle chassis.

The stiffness performance index was derived from the cantilever deflection relationship and is given by Eq. (5).

$$Stiffness\_PI = \frac{\sqrt{E}}{\rho} \tag{5}$$

where $Stiffness\_PI$ is the stiffness performance index, E is Young's Modulus, and ρ is the density of the material.

Since strength also plays a decisive role in frame integrity, a composite performance index was introduced to account for both stiffness and strength while incorporating mass sensitivity. This relationship is given by Eq. (6):

$$Composite\_PI = \frac{\sigma_y \sqrt{E}}{\rho} \tag{6}$$

where $Composite\_PI$ is the composite performance index and σ_y is the yield strength.

Table 2. Mechanical properties and performance indices of candidate materials

SL No	Property	IS 2062 E350	AISI 4130 Chromoly	Aluminum 6061-T6
1	Young's Modulus (GPa)	200	210	68.9
2	Yield Strength (MPa)	350	560	276
3	Density (kg/m³)	7850	7850	2700
4	√E/ρ (Stiffness PI)	1.80	1.84	3.05
5	Composite Index*	796.8	1271.3	384.8

**Higher values indicate a better stiffness–strength–mass balance.*

https://doi.org/10.31436/iiumej.v27i2.4068

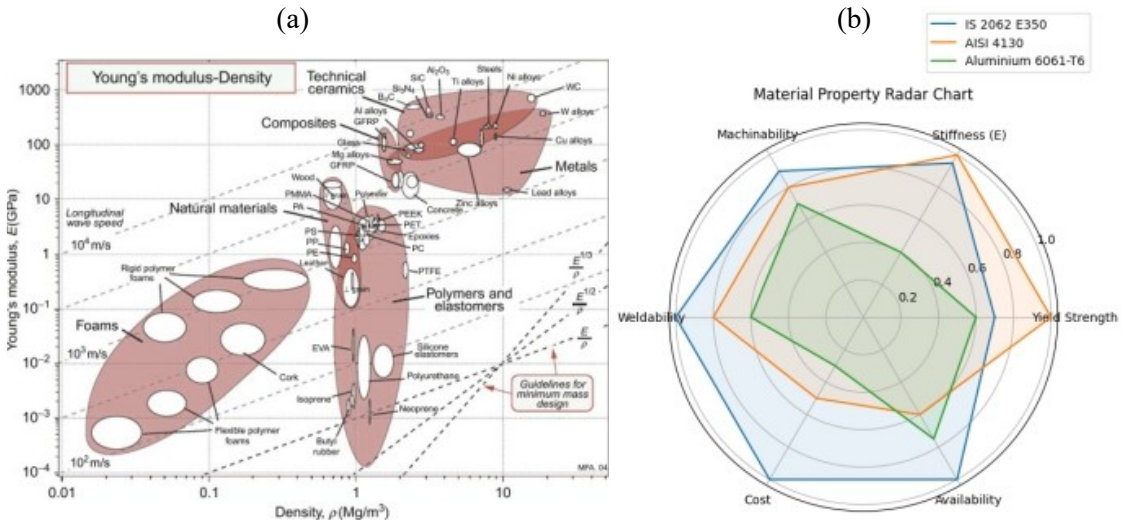

Figure 5. (a) Young's modulus vs. density (Ashby, 2005) (b) Composite Performance Index Radar Chart

The comparative results of these indices are presented in Table 2 and Figure 5b. The evaluation highlights that AISI 4130 exhibits the highest overall performance owing to its superior combination of stiffness and strength. Aluminum 6061-T6 provides an excellent stiffness-to-weight ratio, but its lower modulus limits its resistance to deformation under load. IS 2062 E350 strikes a balanced trade-off among strength, cost, and availability, making it an attractive option for cost-sensitive, large-scale production. While AISI 4130 is technically the most capable material, IS 2062 E350 emerges as a practical choice, particularly in the context of mass manufacturing, where cost and supply-chain accessibility are decisive.

2.5. Finite Element Analysis

Finite Element Analysis (FEA) was carried out in ANSYS Workbench to evaluate the structural performance of the hybrid step-through scooter chassis. Four simulation domains were investigated: static structural, fatigue, impact, and modal analyses to evaluate stiffness, strength, durability, and vibration safety. The chassis was modeled in IS 2062 E350 structural steel, with Aluminum 6061-T6 used as a benchmark for comparative evaluation. The CAD model from SolidWorks was simplified prior to analysis by excluding non-structural parts, such as brackets and fasteners, to reduce computational time.

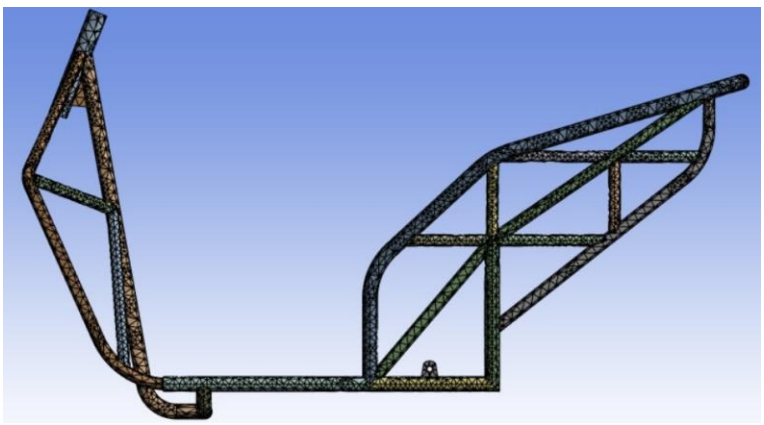

Figure 6. Chassis frame after meshing.

https://doi.org/10.31436/iiumej.v27i2.4068

The frame was meshed using a patch-conforming tetrahedral method. A global element size of 20 mm was adopted, with local refinements of 15 mm applied to four key structural members and a gusset region to better capture local stress concentrations. Further refinement was attempted, but the solver failed to compute beyond this level due to computational resource limits. The final mesh contained approximately 119,161 nodes and 58,220 elements, as shown in Figure 6. This meshing strategy represents a balance between accuracy and computational feasibility.

The boundary conditions for the structural simulation were defined to replicate realistic loading and support scenarios. A fixed support was applied at the rear swingarm mounts, thereby constraining all degrees of freedom at this location. At the headstock, a cylindrical support was introduced to permit both axial and tangential rotation, thereby reproducing the chassis' steering behavior under operating conditions. To evaluate the influence of material properties on overall performance, two material configurations were considered independently in the simulation. The first configuration employed IS 2062 structural steel, while the second utilized Aluminum 6061-T6. This approach enabled a direct comparison of stiffness and stress distribution for the two materials under identical boundary and loading conditions. To maintain conciseness, graphical results are illustrated for steel, while aluminum outcomes are summarized in tables for direct comparison.

2.5.1. Static Structural Analysis

Static analysis quantified the stress distribution and deflection under rider and component loads. Vertical loads corresponding to 1G, 2G, and 3G conditions were calculated using Eq. (1), where m = 100 kg (rider + frame + battery). The resulting loads were distributed across the seat, floorboard, and headstock (Table 3).

Table 3. Load distribution across structural zones

SL No	Zone	Percentage	Load at 1G (N)	Load at 2G (N)	Load at 3G (N)
1	Seat	60%	588.6	1177.2	1765.8
2	Floorboard	25%	245.25	490.5	735.75
3	Headstock	15%	147.15	294.3	441.45

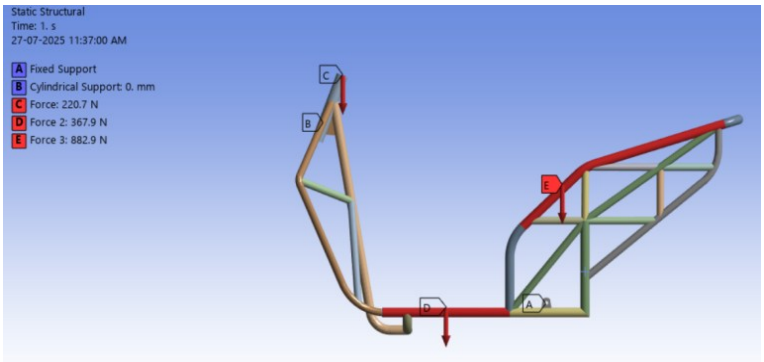

Figure 7. Loads applied to the chassis frame for static analysis.

2.5.2. Fatigue Analysis

Fatigue analysis assessed the long-term durability of the chassis under cyclic loading caused by rider movement, braking, and road-surface irregularities. A cyclic load of 1.5G was applied using the same constraints as in the static analysis. Fatigue life was estimated using the S–N curve approach with Goodman's relation given in Eq. (7)

https://doi.org/10.31436/iiumej.v27i2.4068

$$\sigma_a = \sigma_f'(2N_f)^b \quad (7)$$

Since published S–N data for IS 2062 and 6061-T6 were limited, equivalent literature curves (ASTM A36 structural steel, AA6061-T6 aluminum) were adopted. Missing high-cycle values were extrapolated to 10^8 cycles using standard fatigue trends. For IS 2062 steel, an endurance limit of 160 MPa was used, while aluminum 6061-T6 was evaluated at 95 MPa at 10^7 cycles.

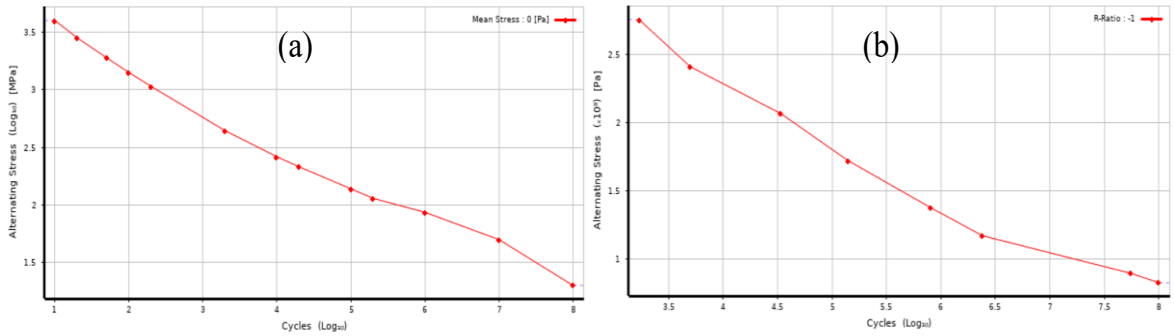

Figure 8. S–N curve for (a) IS 2062 E350 steel and (b) aluminum 6061-T6 alloy

The S–N curves used in fatigue estimation were defined in ANSYS Engineering Data (Figure 8). For IS 2062 E350, alternating stress amplitudes decrease from the order of gigapascals at very low cycles (10–100) to ~50 MPa at 10^7 cycles. For 6061-T6 aluminum, fatigue strength ranged from ~2.75×10^8 Pa at 1.7×10^3 cycles to ~8.27×10^7 Pa at 10^8 cycles, consistent with MIL-HDBK-5H data.

2.5.3. Impact Analysis

Impact loading was modeled using an equivalent static force derived from the work-energy principle. The kinetic energy of the rider–vehicle system was assumed to be absorbed over a prescribed stopping distance. The relationship is given by Eq. (8):

$$F_{eq} = \frac{mv^2}{2d} \quad (8)$$

where m is the effective impact mass, v is the impact velocity, F_{eq} is the equivalent of static impact force, and d is the assumed stopping distance or crush distance. The equivalent impact force ($F_{eq} \approx 1715$ N) was derived from energy conservation using a 100 kg system (rider + vehicle) at 30 km/h (8.33 m/s) and an assumed stopping distance of 0.2 m (conservative for vehicle crush). For conservative localized structural reaction and to match common scooter impact studies, we applied an equivalent static load scaled to represent distributed energy absorption; using an effective force-time conversion and prior literature scaling, the adopted equivalent point load was 1715 N. This approach provides a repeatable, conservative comparative metric while acknowledging limitations versus explicit dynamics.

https://doi.org/10.31436/iiumej.v27i2.4068

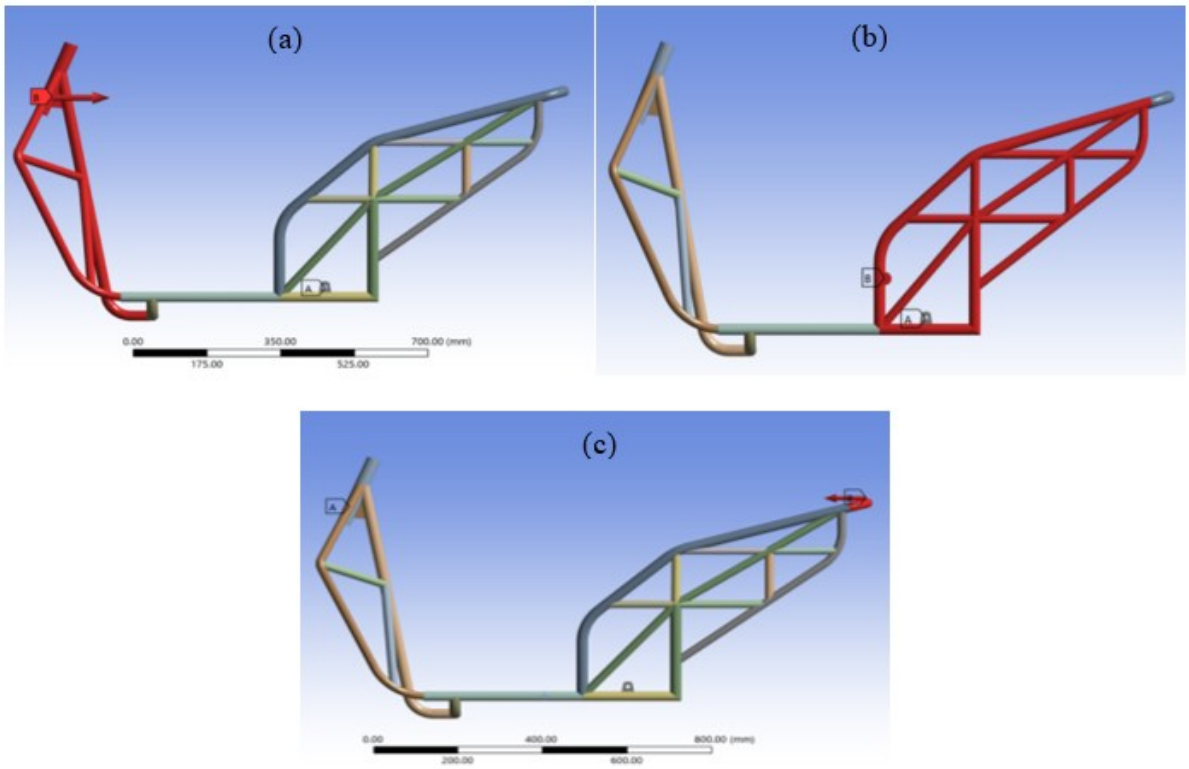

Figure 9. Equivalent static impact load cases: (a) frontal impact at the headstock, (b) side impact at the mid-frame, (c) rear impact at the swingarm mounts.

2.5.4. Modal Analysis

Modal analysis was conducted to extract the first six natural frequencies and corresponding mode shapes of the chassis. The analysis was performed by solving the generalized eigenvalue problem given in Eq. (9):

$$([K] - \omega_i^2[M])\{\phi_i\} = \{0\} \tag{9}$$

where $[K]$ is the global stiffness matrix, $[M]$ is the global mass matrix, ω_i is the i-ith natural circular frequency in rad/s, and $\{\phi_i\}$ is the corresponding mode shape vector.

Modal analysis was performed using the same boundary conditions as the static case (fixed swingarm mounts, cylindrical headstock support). The fundamental mode was identified above 25 Hz, well separated from excitation frequencies due to motor harmonics (~18 Hz) and road input (~15 Hz). This ensures the avoidance of structural resonance during operation.

3. Results and Discussion

3.1. Static Structural Analysis of the chassis

The load-carrying capacity of the chassis was evaluated under vertical accelerations of 1G, 2G, and 3G. Constraints were applied at the rear swingarm mounts (fixed) and the headstock bearings (cylindrical), while loads were distributed across the seat (60%), floorboard (25%), and headstock (15%). The results for the three design iterations using IS 2062 steel are summarized in Table 4.

https://doi.org/10.31436/iiumej.v27i2.4068

Table 4. Static results for design iterations (IS 2062 steel)

Iteration	Load Case	Max Deformation (mm)	Max Stress (MPa)	FOS
	1G	9.56	176	1.99
1	2G	19	352.1	0.99
	3G	28.7	528.1	0.66
	1G	1.66	88.2	3.96
2	2G	3.32	176.4	1.99
	3G	4.98	264.7	1.32
	1G	1.05	78.8	4.44
3	2G	2.11	157.7	2.23
	3G	3.16	236.5	1.48

Iteration 1 showed excessive deformation under 3G loading (28.7 mm) with a FoS < 1, indicating likely permanent deformation. Iteration 2 achieved a substantial reduction in deformation (4.98 mm at 3G) but still exhibited a marginal FoS of 1.32. The final Iteration 3 delivered the most stable performance, limiting deformation to 3.16 mm at 3G while maintaining a FoS of 1.48, thus meeting structural safety requirements. A material benchmarking case at 1.5G is presented in Table 5. Both materials experienced similar stresses (~118 MPa), but aluminum exhibited significantly greater deformation and a lower FoS than steel.

Table 5. Static Analysis at 1.5G for IS 2062 Steel and Al 6061-T6

SL no	Parameter	IS 2062 E350 Steel	6061-T6 Aluminium
1	Total Deformation (mm)	1.5803	4.5813
2	Equivalent Stress (MPa)	118.26	116.08
3	Factor of Safety	2.96	2.38

Overall, Iteration 3 demonstrated the best combination of stiffness and a safety factor, validating the hybrid trellis–step-through configuration for static loading conditions. Steel provided higher stiffness and safety margins than aluminum, while aluminum offered weight reduction at the expense of compliance.

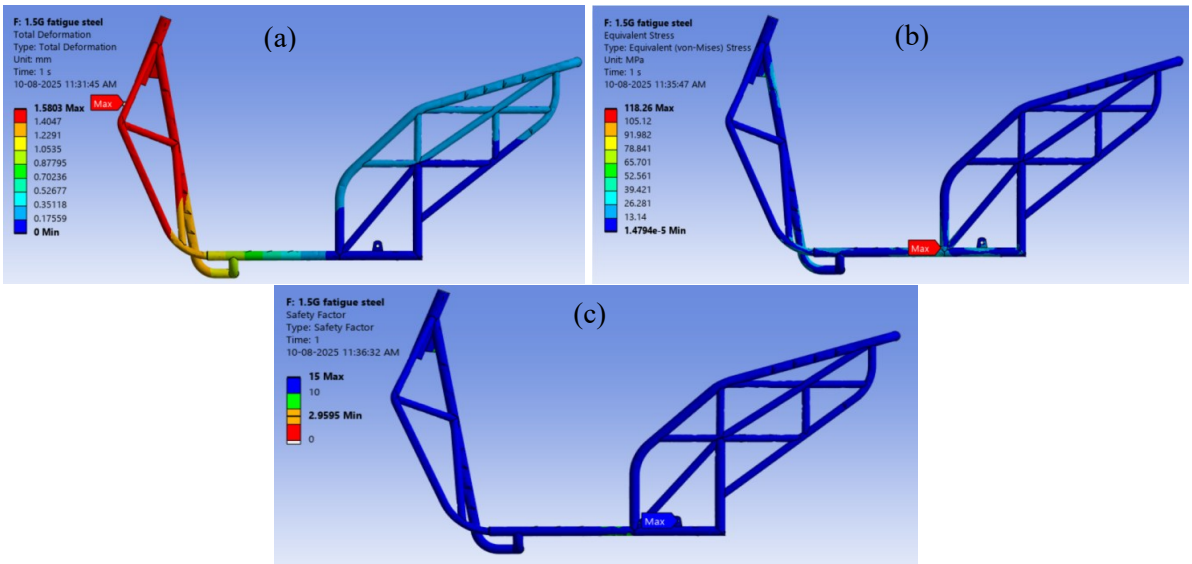

Figure 10. Static analysis of IS 2062 steel under 1.5G load (a) total deformation, (b) equivalent stress, (c) factor of Safety

https://doi.org/10.31436/iiumej.v27i2.4068

3.2. Fatigue Analysis of the Chassis

The fatigue behavior of the chassis was evaluated under 1.5G cyclic loading. The critical regions in the steel frame, particularly around the headstock gussets and swingarm mounts, exhibited the shortest fatigue life. Results for IS 2062 E350 and Aluminum 6061-T6 are shown in Table 6.

Table 6. Fatigue Performance at 1.5G Cyclic Loading

SL no	Parameter	IS 2062 E350	6061-T6 Aluminum
1	Life (cycles)	1.75×10^6	2.73×10^6
2	Factor of Safety	0.423	0.901
3	Damage	57.12	3.67

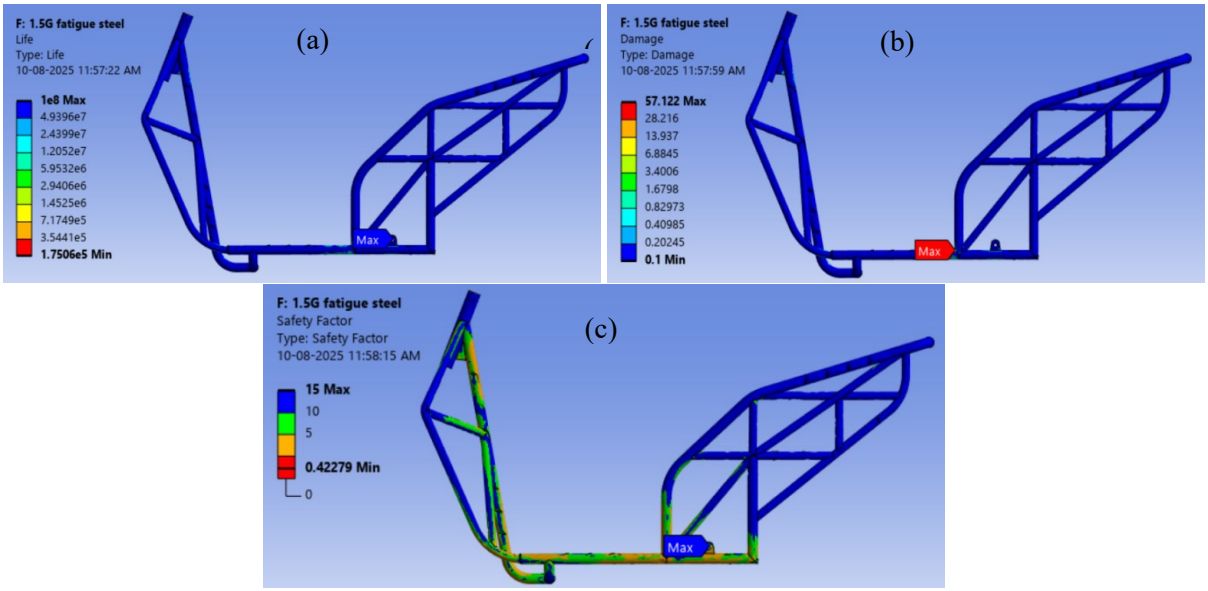

Figure 11. Fatigue analysis of IS 2062 steel under 1.5G load (a) fatigue life, (b) fatigue damage, (c) fatigue factor of Safety

Both materials achieved lives exceeding the design benchmark of 10^6 cycles. Steel exhibited higher stiffness but also accumulated more localized fatigue damage, resulting in a lower fatigue safety factor. Aluminum demonstrated a longer fatigue life and lower cumulative damage, but at the expense of increased deformation. The steel frame met the minimum fatigue life requirements but showed higher susceptibility to local fatigue at welded joints, while the aluminum offered greater fatigue endurance but lower stiffness. A simplified analytical fatigue estimation was also performed using the Goodman mean stress relation to cross-check the simulation results. For IS 2062 E350 steel, assuming an endurance limit of 160 MPa and an alternating stress of ~118 MPa from the 1.5 G static case, the predicted fatigue life was on the order of 1–2 × 10^6 cycles, which agrees well with the FEA minimum of 1.75 × 10^6 cycles. Similarly, for 6061-T6 aluminum, with an assumed endurance stress of ~95 MPa at 10^7 cycles, the method predicted ~2–3 × 10^6 cycles, consistent with the simulation result of 2.73 × 10^6 cycles. This agreement confirms the credibility of the FEA-based fatigue life estimates.

3.3. Impact Analysis of Chassis

Impact performance was evaluated using an equivalent static force of 1715 N applied at three locations: the headstock (front), mid-frame (side), and swingarm pivot (rear).

https://doi.org/10.31436/iiumej.v27i2.4068

All impact scenarios produced stresses exceeding the material yield strength, confirming localized plastic deformation under crash-level conditions. Steel consistently exhibited greater resistance to deformation than aluminum, with the rear trellis acting as a sacrificial energy-absorbing member. Aluminum displayed substantially larger deflections, particularly in frontal and rear impacts. The maximum stresses, deformations, and factors of safety are presented in Table 7.

Table 7. Max Stress, Deformation & FoS under Impact Loading

Material	Location	Max Stress (MPa)	Max Deformation (mm)	Factor of Safety
IS 2062 Steel	Front Impact	2724.2	106.64	0.128
	Side Impact	685.17	8.71	0.511
	Rear Impact	1744.8	106.87	0.2
Al 6061-T6	Front Impact	2689.1	309.24	0.102
	Side Impact	690.01	25.82	0.4
	Rear Impact	1664.7	309.7	0.165

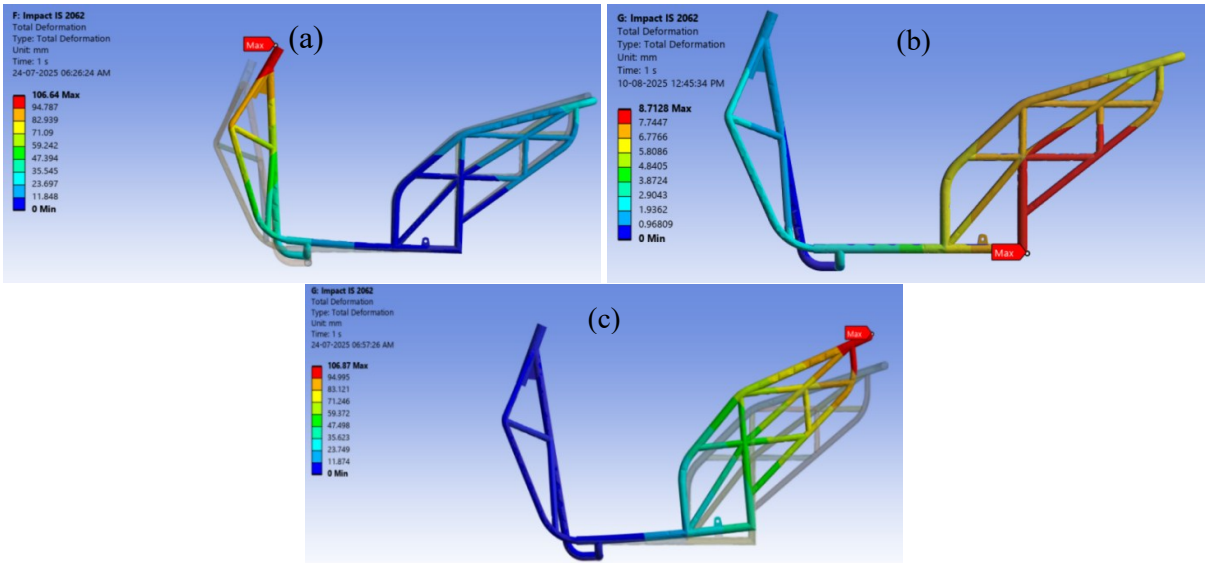

Figure 12. Total deformation of IS 2062 steel at (a) front impact, (b) side impact, (c) rear impact.

Overall, while both materials yielded under extreme loads, the steel chassis maintained structural integrity with more controlled deformations, whereas aluminum exhibited excessive compliance. The impact loading scenario was further validated using a simplified bending stress calculation. Applying the equivalent static load of 1715 N (Eq. 9) over a 0.15 m moment arm gives a bending moment of ~257 N·m. For a Ø26.9 mm × 2 mm tube with a section modulus of approximately 759 mm³, the corresponding bending stress is ~339 MPa. This value exceeds the yield strength of 6061-T6 aluminum and approaches that of IS 2062 E350 steel, in line with the FEA observation of localized plastic deformation under severe impact conditions.

3.4. Modal Analysis of Chassis

The first six natural frequencies and mode shapes of the chassis were extracted, and the results are summarized in Table 8. Figure 13 shows the modal analysis of Mode 1 of 6 modes.

https://doi.org/10.31436/iiumej.v27i2.4068

Table 8. First Six Modal Frequencies & Max Deformation

Mode	Description	Frequency (Hz)	Deformation (mm)	Frequency (Hz)	Deformation (mm)
1	Rear lateral bending (side sway)	28.568	17.027	28.561	29.017
2	Rear vertical bending (up–down)	39.794	22.047	39.486	37.610
3	Global lateral bending (whole chassis)	62.418	16.755	62.346	28.593
4	Rear inward bending (toward centerline)	79.429	23.728	79.386	40.489
5	Global lateral bending (front-dominant)	92.903	15.836	92.863	27.023
6	Rear local torsion (twisting)	155.09	20.331	154.97	34.273

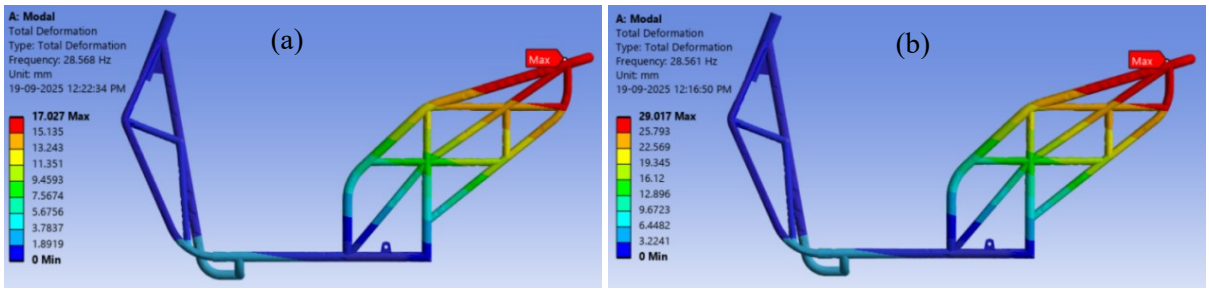

Figure 13. Mode 1 (a) IS 2062 Steel (b) 6061-T6 Aluminum

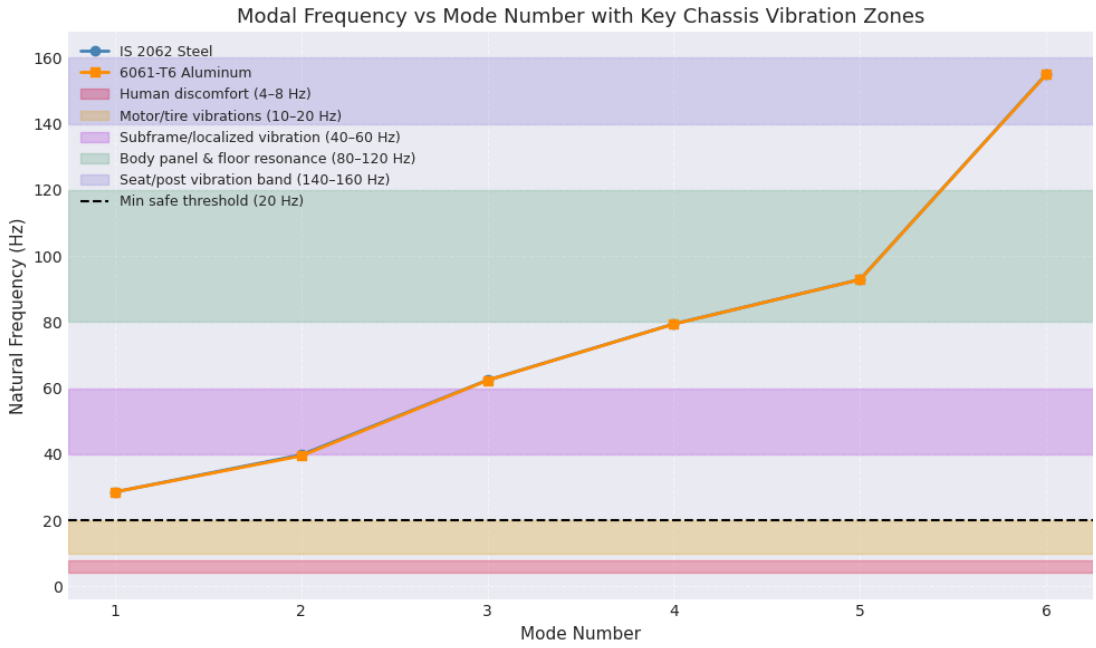

Figure 14. Modal Frequencies with Resonance Zones

For both materials, the fundamental frequency was ~28.6 Hz, well above the typical excitation frequencies from motor harmonics (~18 Hz) and road irregularities (~15 Hz) (Figure 14). Steel exhibited lower modal amplitudes than aluminum, reflecting higher stiffness, and the chassis design successfully avoided resonance in the operational range. An analytical frequency estimation was carried out by approximating the chassis main spine as a cantilever

https://doi.org/10.31436/iiumej.v27i2.4068

beam of length 1.29 m. Using E = 200 GPa, a second moment of area of ~2.9 × 10^4 mm^4 for the primary tube, and an effective end mass of 12 kg, the fundamental bending frequency was estimated at ~26–29 Hz. This closely matches the first mode frequency of 28.56 Hz predicted by FEA for the steel frame, reinforcing the reliability of the numerical modal analysis.

3.5. Discussion

The present hybrid step-through + trellis chassis demonstrates balanced performance across static, fatigue, impact, and modal analyses. In static loading, Iteration 3 limited peak deformation to 3.16 mm at 3G with a FoS of 1.48, confirming that triangulation and gusseting effectively improved stiffness under severe accelerations. Fatigue life under 1.5G cyclic loading reached ~1.75×10^6 cycles for IS 2062 and ~2.73×10^6 cycles for 6061-T6; while steel concentrated damage at welded joints, aluminum showed broader compliance with lower cumulative damage. Impact tests with an equivalent static load of 1715 N produced localized plastic deformation in both materials, but steel consistently controlled displacements more effectively. Modal analysis placed the first natural frequency near 28.6 Hz, well above dominant road and motor excitations, confirming vibration safety. When compared with existing literature, these results show relative advantages, though not direct equivalence. Ajhay Babu (AISI 1020) reported failure under 3G loading with FoS < 1 and unsafe first modes near 10 Hz; by contrast, the present IS 2062 frame remains safe at 3G and dynamically stable. Karthik et al. (AISI 4130) achieved FoS > 2.3 but under lighter impact loads (~650 N), while this study applied nearly triple the load to represent harsher collisions. Composite studies, such as those by Khankal et al., demonstrate fatigue benefits but also face cost and manufacturability issues. These comparisons suggest three categories of prior work: mild steels failing under high loads, high-grade steels validated under lighter impacts, and composites with cost constraints. The present design sits between these extremes—more resilient than mild steel, more realistic in crash assessment than lighter prototypes, and more manufacturable than composites.

Analytical verification further strengthens confidence in the results. A Goodman mean-stress estimate gave fatigue lives on the order of 10^6 cycles for both materials, consistent with FEA predictions. An equivalent bending stress calculation (~339 MPa) explains aluminum's yielding and steel's near-yield behavior under severe impacts. A cantilever beam approximation of the chassis spine predicted a fundamental frequency between 26–29 Hz, matching the 28.6 Hz first mode observed in the FEA. These checks confirm the credibility of the simulation outcomes. In practical terms, the IS 2062 hybrid chassis offers a manufacturable, urban-ready solution. It provides improved high-load tolerance compared with mild steel, avoids resonance across operating conditions, and maintains cost-effectiveness relative to composites or exotic alloys. The integration of trellis reinforcement into both the headstock and rear subframe within a step-through styling envelope represents a novel contribution, combining structural robustness, rider ergonomics, and manufacturability in a configuration suited for mass-market electric scooters. This study used equivalent static impact loads instead of explicit transient crash simulation, and the results are simulation-only, without prototype validation; weld details, fasteners, and manufacturing tolerances were not modeled. Future work should include dynamic crash simulation, welded-joint modeling, prototype fabrication, and instrumented testing to validate and refine the design.

4. CONCLUSION

This study presented the design and structural validation of a hybrid tubular chassis for an electric scooter constrained by a predefined styling envelope. Unlike conventional approaches where geometry dictates styling, the chassis here was required to fit within fixed dimensional

limits while accommodating rider ergonomics. The final design integrated a step-through central spine, a trellis-based rear subframe, and a reinforced headstock, offering a novel structural configuration for scooters. Static analysis showed that the IS 2062 E350 steel frame limited deformation to 3.16 mm at 3G with a factor of safety of 1.48, confirming adequacy under severe urban loads. Aluminum 6061-T6, though lighter, exhibited nearly three times higher deformation and a lower safety margin. Fatigue analysis under 1.5G cyclic loading predicted lives of ~1.75×10^6 cycles for steel and ~2.73×10^6 cycles for aluminum; steel provided higher stiffness but localized fatigue concentration, while aluminum offered greater fatigue endurance but reduced rigidity. Impact analysis revealed that both materials yielded under simulated 30 km/h-equivalent crashes, but steel consistently limited deformations, with the trellis-based rear structure effectively absorbing energy. Modal analysis placed the first natural frequency at 28.56 Hz, well above operational excitation frequencies, eliminating resonance risk; steel also produced lower modal amplitudes than aluminum. Overall, the IS 2062 hybrid frame delivers a manufacturable and robust design that combines stiffness, endurance, and crash tolerance within realistic packaging constraints. The integration of trellis reinforcement into both the headstock and rear subframe while retaining a step-through spine represents a novel contribution to scooter chassis development. Future work should include experimental validation, advanced exploration of lightweight materials, and multi-objective optimization of cost, manufacturability, and ergonomics to further improve practicality.

REFERENCES

[1] Foale, T.: Motorcycle Handling and Chassis Design: The Art and The Science. Tony Foale Designs, Benidoleig (2006). ISBN: 978-84-933286-8-8

[2] Thede, P., Parks, L.: Race Tech's Motorcycle Suspension Bible. Motorbooks, Minneapolis (2010). ISBN: 978-0-7603-3819-3

[3] Balaguru, S., Natarajan, E., Ramesh, S., Muthuvijayan, B.: Structural and modal analysis of scooter frame for design improvement. Mater. Today: Proc. 16, 1106–1116 (2019). https://doi.org/10.1016/j.matpr.2019.05.202

[4] Jeyapandiarajan, P., Kalaiarassan, G., Joel, J., Shirbhate, R., Telare, F.F., Bhagat, A.: Design and analysis of chassis for an electric motorcycle. Mater. Today: Proc. 5(5), 13563–13573 (2018). https://doi.org/10.1016/j.matpr.2018.02.352

[5] Mehra, A., Singh, R., Chauhan, A.S., Nath, K., Yadav, A.: Design and analysis of an electric bike chassis. Mater. Today: Proc. 62, 1510–1520 (2022). https://doi.org/10.1016/j.matpr.2022.02.247

[6] Shivhare, G., Kundu, K., Narayan, J., Dwivedy, S.: Design and modeling of a compact lightweight electric-scooter. In: Proc. IEEE Int. Conf. Computational Performance Evaluation (ComPE), pp. 1–5 (2021). https://doi.org/10.1109/ComPE53109.2021.9752193

[7] Goh, C.P., Chun, T.W.: An in-depth analysis of lightweight chassis design for electric scooters using trellis frame structures. J. Innov. Technol. 30, [pages] (2023). https://doi.org/10.61453/joit.v2023no30

[8] Karthik, K.N., Nandan, M.R., Goudham, B., Abhinand, G.: Design and fabrication of electric motorcycle chassis frame. Int. J. Sci. Res. Eng. Manag. (IJSREM), [pages] (2023). https://doi.org/10.55041/IJSREM26212

[9] Ajhay Babu, J.K.: Design, development and computational finite element analysis (FEA) of an electric two-wheeler frame. Int. J. Res. Appl. Sci. Eng. Technol. (IJRASET) 10(12), 2168–2181 (2022). ISSN: 2321-9653

[10] Shinde, Tarang, et al. "Fatigue analysis of alloy wheel using cornering fatigue test and its weight optimization." Materials Today: Proceedings 62 (2022): 1470-1474. https://doi.org/10.1016/j.matpr.2022.02.023

[11] Rahmadi, A., Mursalin, M.: Design and analysis of chassis frame for chopper-style motorcycle. Media Mesin: Maj. Tek. Mesin 25(1), 64–76 (2024). https://doi.org/10.23917/mesin.v25i1.3224

[12] Srinu, V., Sarma, V.M., Gopal, K.G., Varma, N.M., Vyas, G.: Design and computational analysis of chassis frame for electric bike. J. Emerg. Technol. Innov. Res. (JETIR) 8(6), [pages] (2021). ISSN: 2349-5162

[13] Teja Sri, C., Naga Gowtham Kumar, M., Madhuri, B.V.S.A., Komali Harika, G., Sateesh, B.: Design and development of electric moped chassis. In: Proc. Indian Int. Conf. Industrial Engineering and Operations Management (IEOM), Warangal, India. IEOM Society International, pp. [pages] (2022)

[14] Vashist, D., Singh, N., Tomar, G., Shadija, A.S.: Design analysis of electric two wheeler frame. Proc. IEI Conf., [pages] (2021). https://doi.org/10.36375/prepare_u.iei.a243

[15] Biswal, B., Setiadi, R., Kriswanto, K., Arif, B.: Design and fabrication of electric bike with sliding frame. J. Appl. Eng. Sci. 19(4), 948–953 (2021). https://doi.org/10.5937/jaes0-28957